Journal of Materials Chemistry C

ROYAL SOCIETY OF CHEMISTRY

PAPER

View Article Online
View Journal | View Issue

Cite this: J. Mater. Chem. C, 2025, 13, 19778

Harnessing substituent and aggregation-induced effects for color-tunable emission in borafluorenium ions

Nathan C. Frey, [a] Kimberly K. Hollister, [a] Caleb C. Taylor, [b] Nula Jones, [b] Diane A. Dickie [b] and Robert J. Gilliard Jr *[a]

Received 22nd July 2025,
Accepted 22nd August 2025

DOI: 10.1039/d5tc02785c

rsc.li/materials-c

Once considered a "laboratory curiosity", cyclic borenium ions have recently been shown to exhibit tunable emission and stimuli-responsive properties. Utilizing hexaphenylcarbodiphosphorane (CDP), a series of borafluorenium and 3,3′-dimethoxyborafluorenium ions were synthesized to determine the impacts of counteranion and substituent effects on the optical properties and stability of borafluorenium ions. Clear relationships were established between structure and properties, with emission wavelengths of the borafluorenium ions ranging from yellow (λ_{em} = 559 nm) to red (λ_{em} = 650 nm). By employing density functional theory, a possible mechanism for the observed luminescent behavior was proposed. These compounds were shown to exhibit aggregation-induced emission (AIE) properties and significant changes in solid-state emission color when compared to those observed in solution. The AIE properties of a CDP–borafluorenium ion with dimethoxy substitution were further explored by perturbing the temperature in solution, which resulted in a clear shift in emission wavelength from 563 nm (yellow, 20 °C) to 513 nm (green, −90 °C).

Introduction

Isoelectronic to carbocations, tricoordinate organoboranes have been employed as key components of functional materials, such as non-linear optics[1–4] and organic light-emitting diodes (OLEDs).[5–9] As such, there have been widespread efforts towards the utilization of tricoordinate boracycles as a key component in conjugated systems, namely polycyclic aromatic hydrocarbons (PAHs).[10–15] The incorporation (or "doping") of boron into PAHs has been shown to significantly stabilize the energy of the lowest unoccupied molecular orbital (LUMO) of the molecule compared to its carbonaceous analogues.[16] Moreover, due to the prominent p–π* conjugation of the tricoordinate boron center with the surrounding conjugated scaffold, the luminescent properties of boron-containing heterocycles can be significantly altered by chemical modification at the boron center. Among the variety of known boron-centered species, tricoordinate boron cations (more commonly known as borenium ions) have emerged as promising candidates for luminescent materials owing to their tunable electronic properties, lower LUMO energies compared to their neutral analogues, and stimuli-responsive behavior. Recent studies by our group[17–22] and others[23–25] have highlighted the versatility and potential of borenium ions for advanced molecular and solid-state materials applications. Despite this, studies on the optical properties of borenium ions remain limited compared to their neutral analogues due to their pronounced reactivity and need for stabilization through methods other than solely kinetic protection (*e.g.*, installation of a bulky substituent).

One commonly utilized strategy to isolate reactive borenium ions is through coordination of neutral, Lewis basic ligands, such as N-heterocyclic carbenes (NHCs).[17–21,24,26–29] Although these ligands provide some degree of kinetic stability to the borenium center, carbene coordination alone has been shown to insufficiently stabilize borafluorenium ions towards aerobic conditions.[17,20] Whereas carbene ligands possess formal carbon(II) centers that donate electron density through one lone pair of electrons in a σ fashion, carbone ligands feature carbon(0) centers that allow for σ and π donation, thereby providing thermodynamic stabilizing effects in conjunction with bulky periphery groups that provide kinetic stabilization.[30–42] Although carbone-stabilized acyclic borenium ions have been investigated since 2011,[43–46] our laboratory has more recently disclosed that carbone ligands bestow exceptional stability to cyclic borenium ions while unlocking various luminescent properties, including aggregation-induced emission (AIE)[18,20]

[a] Department of Chemistry, Massachusetts Institute of Technology, 77 Massachusetts Avenue, Building 18-596, Cambridge, MA 02139-4307, USA. E-mail: gilliard@mit.edu
[b] Department of Chemistry, University of Virginia, Charlottesville, Virginia 22904, USA

and twisted intramolecular charge transfer (TICT)[18] processes. To begin to understand the root cause of these attributes, the synthesis, bonding, and initial photophysical properties of carbone-stabilized borafluorenium,[18,21] azaboracenium,[19] and borepinium[20] ions have been investigated. However, the field of luminescent borenium ions remains in infancy.[22]

The reports of luminescent borenium ions have categorized these systems into a class of fluorophores that display stimuli-responsive changes in emission, which have proven to be desirable due to their applications in various sensing[47–50] and security-relevant fields.[51–54] Among the stimuli-responsive behaviors that these compounds exhibit is thermochromism,[55,56] in which the emission color is responsive to the specific temperature of the sample. Although conventional organic fluorophores commonly exhibit aggregation-caused quenching (ACQ),[57] whereby the fluorescence of a luminophore is quenched at high concentrations, there has been a widespread effort to develop compounds that portray AIE properties,[58–60] which have been utilized for OLED[61] and biosensor[62,63] applications. Due to the pseudo-double bond character between the carbon and boron centers in carbone-ligated borafluorenium ions, parallels of this motif can be drawn with the ubiquitous AIEgen tetraphenylethylene (TPE),[64] particularly in the hindered substituents peripheral to the central double bond of each (Fig. 1). Numerous studies have been performed to analyze the photophysical properties of TPE-like structures, such as diphenylbenzofulvene[65,66] and iminoborane,[67,68] yet studies of systems containing B=C motifs are significantly less explored for this purpose due to their often-highly reactive nature.[69]

Herein, we report the synthesis of carbodiphosphorane-stabilized 9-borafluorenium (**1**, **2**) and 3,3′-dimethoxy-9-borafluorenium (**4**, **5**) ions that exhibit clear structure–property relationships as a function of substituent incorporation and counteranion identity. These properties are exemplified by pronounced shifts in emission wavelength ranging from yellow (λ_{em} = 559 nm) to red (λ_{em} = 650 nm). The compounds were then subjected to studies of the AIE properties, which are proposed to be caused by restricted intramolecular motion (RIM), including suppression of the carbone–boron bond rotation. These borenium ions exhibit the highest AIE factors of any borenium ion to date (with values up to 52.21), as well as pronounced shifts in λ_{em} from the solution-state to solid-state. Photophysical data are supported by density functional theory (DFT) calculations that describe the destabilizing effects on the frontier molecular orbitals due to substituent modification. DFT is also employed to propose a mechanism for the pronounced Stokes shifts observed in the borafluorenium ions. Compound **5**, which comprises dimethoxy substituents and a tetrakis[3,5-bis(trifluoromethyl)phenyl]borate counteranion, notably displays changes in emission wavelength from 563 nm (20 °C) to 513 nm (−90 °C) in toluene, yielding temperature-responsive behavior. Our results demonstrate the powerful role of aryl functionalization and counteranion selection in controlling the stability and electronic properties of highly emissive borafluorenium ions while providing critical insight into designing next-generation luminescent borenium ions for advanced applications.

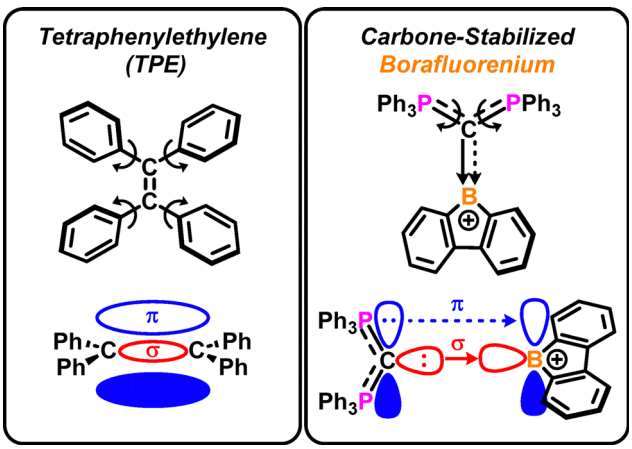

Fig. 1 Analogy between tetraphenylethylene (TPE, left) and carbone-stabilized borafluorenium ion (right). Curved arrows represent bonds with restricted rotations; dashed arrows represent non-ideal π-overlap between the carbone ligand and boron p_z orbital due to geometric constraints.

Results and discussion

The combination of equimolar amounts of 9-bromo-9-borafluorene[70] and hexaphenylcarbodiphosphorane (CDP)[30] in toluene results in a nucleophilic displacement reaction of the bromide, leading to isolation of the CDP–ligated borafluorenium ion **1** in 88% yield as a pale yellow solid (Scheme 1). Compound **1** exhibits an $^{11}B\{^1H\}$ NMR shift at 57.7 ppm, indicative of a tricoordinate cationic boron center, as well as a $^{31}P\{^1H\}$ resonance at 24.6 ppm. In order to access a CDP–borafluorenium ion with an alternative counteranion, 9-bromo-9-borafluorene was combined with an equimolar amount of CDP in toluene, followed by addition of an equimolar amount of sodium tetrakis[3,5-bis(trifluoromethyl)phenyl]borate ($NaBAr^F_4$) in *o*-difluorobenzene (*o*-DFB), which yielded borafluorenium ion **2** as a pale green solid (58% yield). The $^{11}B\{^1H\}$ NMR spectrum of **2** shows two resonances: 57.6 ppm (corresponding to the borafluorenium center) and −6.6 ppm (corresponding to the BAr^F_4 counteranion). To determine the effects of counteranion identity on the photophysical properties of carbone-stabilized borafluorenium ions, we then sought to analyze the optical properties of compounds **1** and **2** using various spectroscopic methods. During this process, it was discovered that **1** and **2** both experience photosensitivity (*vide infra*). Therefore, inspired by our previous report of thermochromic 3-methoxy-9-borafluorenium ions,[17] among additional reports of functional group installation by various research groups,[71–78] we envisioned that dual incorporation of π-donor substituents onto the aryl backbone of the 9-borafluorene unit could impart stability towards and modify the photophysical properties of these borafluorenium ions.

Lithiation and borylation of 2,2′-dibromo-5,5′-dimethoxybiphenyl[79] resulted in the formation of 3,3′-dimethoxy-9-bromo-9-borafluorene (**3**) as a yellow solid in 33% yield. The low yield is

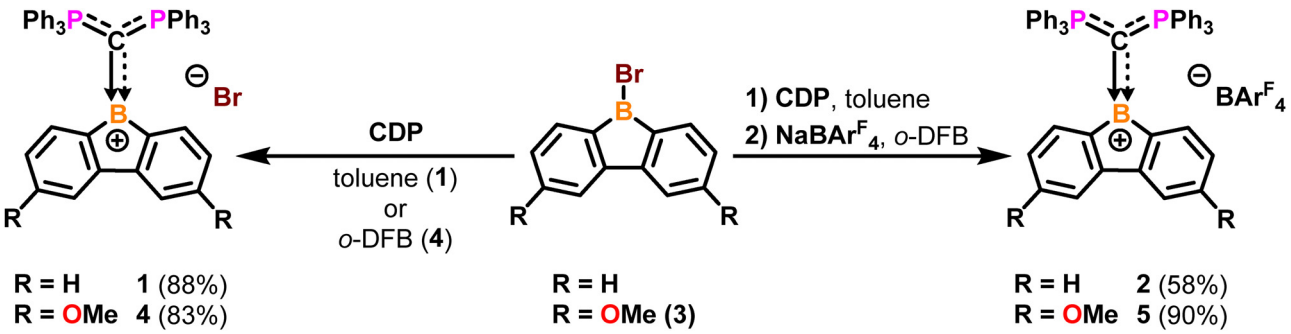

Scheme 1 1 Synthesis of hexaphenylcarbodiphosphorane (CDP)-stabilized borafluorenium ions from 9-bromo-9-borafluorene or 3,3′-dimethoxy-9-bromo-9-borafluorene (**3**). BAr^F_4 = tetrakis[3,5-bis(trifluoromethyl)phenyl]borate; *o*-DFB = 1,2-difluorobenzene.

speculated to be complicated by methoxy coordination to boron tribromide during the borylation process. Formation of the boracycle was evident by $^{11}B\{^1H\}$ studies, which indicated the presence of a tricoordinate boron center at 61.9 ppm. This resonance is upfield-shifted from 9-bromo-9-borafluorene (δ = 65.8 ppm)[80] and 3-methoxy-9-bromo-9-borafluorene (δ = 63.6 ppm),[17] indicating that the boron of **3** is slightly more electron-rich than the latter two species. Combination of one equiv. of CDP and **3** in *o*-DFB led to the isolation of **4** as a pale-yellow solid in 83% yield (Scheme 1). Similar to the synthesis of **2**, addition of $NaBAr^F_4$ to equimolar amounts of **3** and CDP in a toluene/*o*-DFB mixture led to the formation of a pale-green suspension that was isolated as compound **5** in 90% yield after workup. The $^{11}B\{^1H\}$ resonance of **4** (54.3 ppm) and **5** (56.9 ppm) are expectedly upfield-shifted from **1** (57.7 ppm), due to the increased donation from the methoxy substituents. The $^{11}B\{^1H\}$ and $^{31}P\{^1H\}$ resonances for the **1**, **2**, **4**, and **5** are consistent with previously reported CDP-borenium ions.[20,43,45,46]

Single crystals suitable for X-ray diffraction of **1** were grown from the slow diffusion of diethyl ether (Et_2O) into dichloromethane (DCM) at room temperature, which afforded yellow plate-like crystals, while green, block-like crystals of **2** and **5** were grown from vapor diffusion of pentane into concentrated *o*-DFB solutions (Fig. 2). Yellow needle-like single crystals of the neutral 3,3′-dimethoxy-9-bromo-9-borafluorene (**3**) were grown from concentrated toluene at −37 °C. Due to the poor solubility of appreciable amounts of **4** in all screened solvents, including dichloromethane, acetonitrile, toluene, and *o*-DFB, single crystals of this species could not be isolated. The solid-state structures of **1**, **2**, and **5** confirm that each species exists as charge-separated cation–anion pairs (Fig. 2). The $^{carbone}C$–B (C13–B1) bond in **1** (1.519(4) Å) is shorter than those observed in **2** (1.535(3) Å) and **5** (C15–B1; 1.539(3) Å), suggesting that counteranion identity and methoxy-substitution play a role in the C–B bond length. These results are further corroborated by

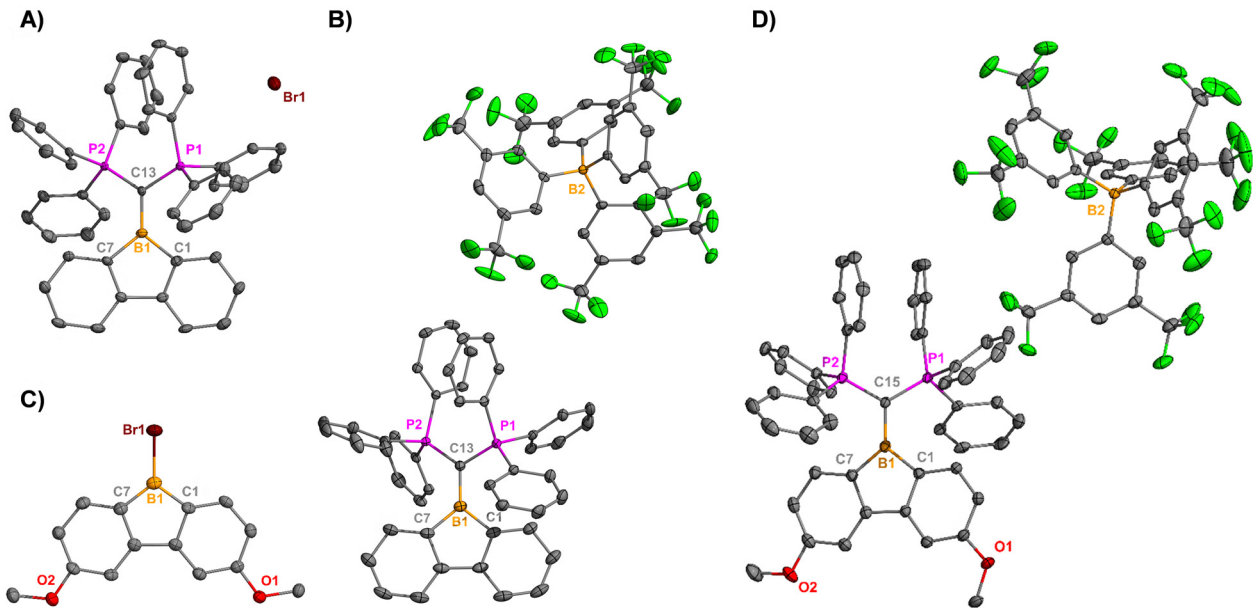

Fig. 2 Molecular structures of **1** (A), **2** (B), **3** (C) and **5** (D); hydrogen atoms and solvent molecules (**5**) are omitted for clarity. Anisotropic displacement parameters are depicted at 50% probability level and only the major position of any disordered atoms is shown. Selected distances (Å): **1**: B1–C13: 1.519(4); P1–C13: 1.754(3); P2–C13: 1.749(3); **2**: B1–C13: 1.535(3); P1–C13: 1.757(2); P2–C13: 1.753(2); **3**: B1–Br1: 1.924(5); **5**: B1–C15: 1.539(3); P1–C15: 1.7411(18); P2–C15: 1.7398(17).

Table 1 Absorption, emission, quantum yield, and lifetime data for compounds **1**, **2**, **4**, and **5** in DCM, solid, and polycrystalline film states

	λ_{max}	λ_{em} (DCM[a]|solid|film[b])	Φ_F (DCM[c]|solid|film)	α_{AIE}[d]	τ_s/ns (DCM|solid|film)
1	340 nm	650 nm|490 nm|506 nm	0.013|0.680|0.233	52.21	4.29 (100%)|16.86 (5.6%), 46.08 (94.4%)|5.91 (6.9%), 39.84 (93.1%)
2	340 nm	640 nm|500 nm|504 nm	0.024|0.733|0.496	30.54	4.18|56.26 (5.5%), 160.45 (94.5%)|13.13 (7.5%), 72.99 (92.5%)
4	340 nm	559 nm|524 nm|528 nm	0.046|0.574|0.400	12.48	10.07 (71.5%), 191.07 (28.5%)|9.34 (1.3%), 89.71 (98.7%)|14.54 (5.4%), 70.92 (94.6%)
5	340 nm	563 nm|517 nm|523 nm	0.083|0.724|0.400	8.72	9.90 (100%)|30.67 (5.5%), 149.65 (94.5%)|21.92 (4.9%), 121.92 (95.1%)

[a] 0.01 mM. [b] Polycrystalline film was prepared by dropcasting a 10 mM solution of each sample in DCM onto a quartz substrate. [c] Solution-state Φ_F values were collected at 0.001 mM concentrations. [d] $\alpha_{AIE} = \frac{\Phi_F^{solid}}{\Phi_F^{solution}}$.

analysis of Wiberg bond indices (WBI) of $\mathbf{1}^+$ and $\mathbf{4}^+$ (counteranions not considered), which indicate that the WBI for the ^{carbone}C–B bond decreases from 1.05 ($\mathbf{1}^+$) to 1.00 ($\mathbf{4}^+$). Due to the steric bulk of the CDP ligand, intermolecular π-stacking interactions are not observed in the solid-state structures of **1**, **2**, or **5**. The B1–Br1 bond distance in **3** (1.924(5) Å) is similar to those reported for 9-bromo-9-borafluorene (1.909(10) Å).[81]

The photophysical properties of **1**, **2**, **4**, and **5** were studied in detail using various spectroscopic techniques (Table 1). Each borenium ion exhibits markedly similar absorption profiles with λ_{max} for each compound observed at 340 nm (Fig. 3) in DCM. Although $\mathbf{1}^+$ and $\mathbf{4}^+$ possess nearly identical HOMO–LUMO gaps (3.80 eV for $\mathbf{1}^+$; 3.76 eV for $\mathbf{4}^+$), incorporation of the 3,3′-dimethoxy functional groups in $\mathbf{4}^+$ result in destabilization of both the HOMO and LUMO energy levels (Fig. S53). In DCM, compounds **1** and **2** exhibit lowest-energy emission processes (λ_{em}) at 650 nm (**1**) and 640 nm (**2**), which are bathochromically-shifted compared to **4** (559 nm) and **5** (563 nm). The high-energy emission peaks in all compounds are due to small amounts of decomposition at low concentrations that cannot be avoided, even in the presence of rigorously dried and freshly distilled solvent, as confirmed by excitation spectra and concentration- and excitation-dependent emission scans (Fig. S35). However, these results also confirm that the lowest-energy emission band is attributed to the borafluorenium ion. Compounds **1** and **2** display large Stokes shifts (14 000 cm^{-1} for **1**, 14 000 cm^{-1} for **2**) in solution, which suggest significant structural deviation in the excited state (*vide infra*). However, the Stokes shifts of **4** (12 000 cm^{-1}) and **5** (12 000 cm^{-1}) are smaller, indicating some degree of similarity between the ground state and excited state geometries. These data suggest that methoxy substitution plays a significant role in the excited state electronic structure by rigidifying the excited state geometry, while the counteranion appears to have

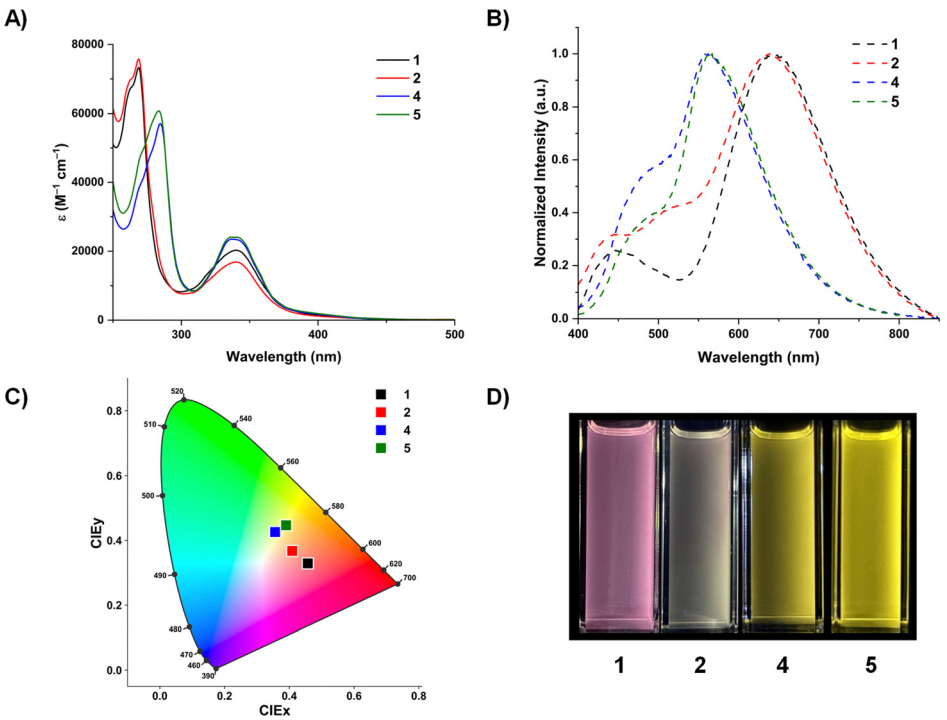

Fig. 3 (A) UV-Vis spectra of **1**, **2**, **4**, and **5** in DCM (0.01 mM) at room temperature. (B) Normalized fluorescence spectra of **1**, **2**, **4**, and **5** in DCM (0.01 mM) at room temperature (λ_{ex} = 340 nm). (C) CIE (1931) chromaticity diagram of **1**, **2**, **4**, and **5** in DCM (0.01 mM) at room temperature. (D) Images of **1**, **2**, **4**, and **5** in DCM (1 mM) under 365 nm light.

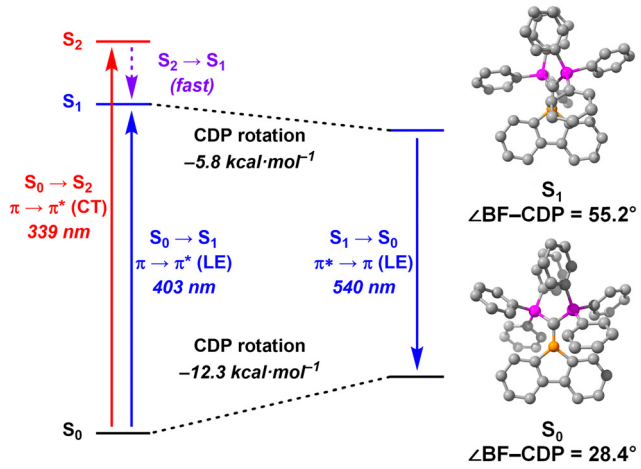

Fig. 4 Potential energy diagram for $\mathbf{1}^+$ computed at the CPCM(DCM)-B3LYP-D3(BJ)/def2TZVP (for S_0) and CPCM(DCM)-TD-B3LYP-D3(BJ)/def2TZVP (for S_1) levels of theory.

a limited effect. All compounds exhibit low Φ_F values (<0.100) in solution (Table 1), which can be explained by the molecules undergoing non-radiative decay pathways, such as B–C and C–C bond rotations, which are more prominent in the solution state than in the bulk solid or film states (Table S1). Moreover, Φ_F values increase with methoxy functionalization and anion exchange from Br^- to BAr_4^{F-}. The dependence of Φ_F on counter-anion identity is proposed to be the result of external heavy atom quenching in **1** and **4**.[82,83] Moreover, the large anion volume of BAr_4^{F-} can discourage non-radiative pathways as a result of intermolecular interactions in solution.[84,85] Interestingly, the fluorescence lifetime (τ_s) of compounds **1** and **2** are significantly shorter than those of compounds **4** and **5**, indicating that the dimethoxy substitution has a direct impact on these values, which has been observed for other methoxy-substituted flurophores.[86–88] While **4** portrays biexponential decay in solution state, **1**, **2**, and **5** each exhibit monoexponential decay pathways.[87,88]

To provide insight into the dynamics of the dimethoxy functionalities, the OMe rotational barriers were computed at the CPCM(DCM)[89]-B3LYP[90,91]-D3(BJ)[92]/def2TZVP[93] level of theory. The free energy profile (Fig. S55) revealed that the rotation is limited by a transition state of $\Delta G^{\ddagger} = +4.3$ kcal mol^{-1}, which is easily accessible at room temperature. TD-DFT analysis of $\mathbf{1}^+$ and $\mathbf{4}^+$ at the CPCM(DCM)-TD-B3LYP-D3(BJ)/def2TZVP level of theory show that the $S_0 \rightarrow S_1$ transitions exhibit forbidden ($f < 0.01$) local excitation (LE) $\pi \rightarrow \pi^*$ (HOMO $\rightarrow$ LUMO) characteristics, which corroborates the tailing effects observed in the absorbance spectrum of both species. However, the $S_0 \rightarrow S_2$ transition for $\mathbf{1}^+$ ($\pi \rightarrow \pi^*$; HOMO-1 $\rightarrow$ LUMO; $f = 0.33$) and $S_0 \rightarrow S_3$ transition for $\mathbf{4}^+$ ($\pi \rightarrow \pi^*$; HOMO-1 $\rightarrow$ LUMO; $f = 0.45$) are each symmetry-allowed charge transfer (CT) transitions. Employing a four-point approach for reorganization energy at the CPCM(DCM)-TD-B3LYP-D3(BJ)/def2TZVP level of theory, a mechanism for state-specific absorption and emission processes is proposed (Fig. 4 for $\mathbf{1}^+$, Fig. S64 for $\mathbf{4}^+$). The $S_0 \rightarrow S_1$ transition for $\mathbf{1}^+$ is computed to be 403 nm but is not observed experimentally due to the forbidden nature of the transition. The computed absorbance from $S_0 \rightarrow S_2$ (341 nm) agrees with the experimentally observed λ_{max} (340 nm). Internal conversion from S_2 to S_1 is presumed to be a fast process ($\Delta E_{S_2-S_2} = 0.581$ eV). The S_1 geometry of $\mathbf{1}^+$ indicates a twisting of the carbone–borafluorene bond, with the torsion angle changing from 28.4° (S_0) to 55.2° (S_1) ($\Delta E_e = -5.8$ kcal mol^{-1}) and is similar to our previously observed twisted intramolecular charge transfer (TICT) process in carbodicarbene(CDC)–borafluorenium ions.[18] An elongation in the carbone–borafluorene bond elongation from 1.519 Å (S_0) to 1.567 Å (S_1) is also observed. Due to the occupied frontier orbitals of CDP being lower in energy than CDC, the CDP has minimal contribution to the $S_0 \rightarrow S_1$ transitions for $\mathbf{1}^+$ and $\mathbf{4}^+$, which not only results in $S_0 \rightarrow S_1$ being almost purely LE in character, but it also precludes TICT processes in these lower energy states. From the relaxed S_1 geometry, $\mathbf{1}^+$ emits a photon (540 nm) and electronically relaxes to S_0, which then converts to the local minimum on the S_0 surface ($\Delta E_e = -12.3$ kcal mol^{-1}).

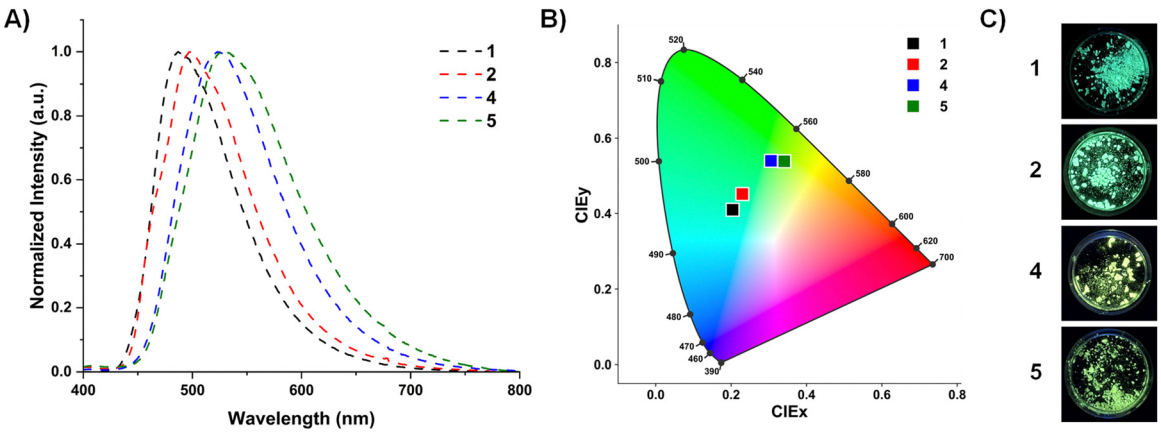

Fig. 5 (A) Normalized solid-state emission spectra of **1**, **2**, **4**, and **5** (λ_{ex} = 340 nm). (B) CIE (1931) chromaticity diagram of **1**, **2**, **4**, and **5** in the solid-state. (C) Images of **1**, **2**, **4**, and **5** in the solid-state under 365 nm light.

The fluorescence quantum yields of compounds **1**, **2**, **4**, and **5** are very low in DCM, indicating minimal emission in the molecularly dispersed state. However, upon transition to the solid state, all four compounds exhibit a substantial enhancement in Φ_F. These observations imply that CDP-coordinated species exhibit aggregation-induced emission (AIE) behavior,[58–60] echoing our previous findings on CDC-borenium ions.[18,20] The AIE factor (α_{AIE}), defined by the equation $\alpha_{AIE} = \frac{\Phi_F^{solid}}{\Phi_F^{solution}}$, is a quantification of the AIE properties of a molecule. Notably **1**, **2**, **4**, and **5** exhibit the highest α_{AIE} values of any borenium ions to date, with **1** the highest value (52.21), followed by **2** (30.54), **4** (12.48), and **5** (8.72). The high α_{AIE} are proposed to be caused by a combination of the suppression of non-radiative pathways in the solid-state and the high degree of overlap in the LE process of these borenium ions. As seen in solution, compounds **2** and **5** exhibit higher Φ_F values than **1** and **4** due to the bulkier BAr_4^{F-} counteranion precluding interactions between fluorophores, even in the aggregate state.[94,95] While **1** and **2** appear blue-green in the solid-state under 365 nm light, compounds **4** and **5** exhibit yellow-green fluorescence (Fig. 5A–C). The pronounced rigidity of these species in the solid-state is believed to suppress non-radiative decay pathways, resulting in a bathochromic shift in λ_{em} compared to that observed in solution. Moreover, the rigidity of these systems in the solid-state, combined with inhomogeneity within the solid sample, can lead to multi-exponential decay pathways. The more Gaussian-like emission profile when compared to the solution-state is attributed to higher stability of the compound in the solid-state. Polycrystalline thin films of **1**, **2**, **4**, and **5** show similar fluorescence data to those observed in the solid-state (Table 1 and Fig. S36). As such, the AIE properties of **1**, **2**, **4**, and **5** can be ascribed to the TPE-like structure of the carbone-boron pseudo double bond, preclusion of intermolecular π–π interactions, and the elongation of $C^{carbone}$–B bond and rotation of the carbone ligand in the excited state (*vide supra*).[96] The hypsochromic shift in λ_{em} and increased Φ_F from solution state to solid state is attributed to restricted intramolecular motion (RIM).[97] First termed by Tang in 2011, RIM results in the AIE properties of molecules, such as TPE, wherein non-radiative molecular rotations are suppressed as a function of physical constraint, such as solvent viscosity, low temperature, or aggregation.[98,99] Interestingly, all compounds exhibit longer fluorescence lifetimes, each possessing multiexponential decays, in the bulk solid and film states than in solution. This trend is ascribed to the suppression of the non-radiative pathways that occur in solution.

We then sought to determine if the dimethoxy substitution in **4** and **5** results in increased stability of the borafluorenium ions when compared to **1** and **2**. By analyzing the percent change in absorbance at 340 nm (Δ_{abs}) as a function of the number of emission scans run on a single sample, it was determined that compounds **1** and **2** exhibit photosensitive properties, with Δ_{abs} decreasing by 8.38% (**1**) and 45.7% (**2**) after 50 emission scans (λ_{ex} = 340 nm) (Fig. S41). Conversely, there is a negligible change in Δ_{abs} observed for compounds **4** (Δ_{abs} = −2.60%) and **5** (Δ_{abs} = −3.87%) after 50 emission scans (λ_{ex} = 340 nm), illustrating the stabilizing effects of π-donating substituents on the boron center. Moreover, analysis of UV-vis spectra over the course of 720 minutes showed that, although compound **1** is more photostable than **2**, **1** is significantly less stable in the dark in DCM ($t_{1/2}$ = 7.9 hour) than **2** ($t_{1/2}$ = 105.5 hour) at 0.01 mM concentrations. In accordance with the photostability studies, compounds **4** ($t_{1/2}$ = 150.2 hour) and **5** ($t_{1/2}$ = 137.5 hour) exhibit exceptional stability in solution compared to **1** and **2**, even at low concentrations, providing further evidence of substituent-induced stability. These data indicate that, although the choice of counteranion has some impact on the stability of the cation, the largest contribution to increased stability arises from the incorporation of electron-donating substituents. The higher stability of **4** and **5** in solution is proposed to arise from the donation of oxygen lone pairs into the vacant p_z orbital of the borenium center, which increases electron density at the boron and therefore reduces its electrophilicity. Interestingly, compounds **1** and **4** were shown to be significantly less stable in the solid-state when exposed to air compared to **2** and **5** with decomposition of **1** and **4** proceeding within three days under air. These data suggest that the bulkier BAr_4^{F-} counteranion contributes significantly to improving the solid-state stability when compared to the smaller Br^- ion in these systems.

In attempts to further elucidate the AIE properties of these borenium ions, we attempted to perform a systematic study on aggregate formation as a function of tetrahydrofuran (THF):water fractions (f_{water}). Due to the σ and π-donation from carbodiphosphorane to borafluorene, all compounds are stable towards THF, which often coordinates to, or is ring-opened by, tricoordinate boracycles.[100,101] Attempts to perform THF : water AIE studies with **1** and **4** were impeded by the poor solubility of both species in THF. Although **2** did form aggregates at a 1 : 99 THF : water ratio, the aggregates visibly decomposed within minutes, with a change in fluorescence color from blue-green to blue. However, the pronounced solubility and stability of **5** enabled the execution of systematic AIE studies. Similar to its behavior in DCM and toluene (*vide infra*), **5** exhibits an absorbance feature at 337 nm and a fluorescence feature at 561 nm in neat THF (f_{water} = 0%). At very high water content (f_{water} = 99%), **5** formed a stable suspension exhibiting bright green fluorescence due to the immediate formation of a colloidal suspension preventing interactions with water. Investigation of the absorbance profile of this species shows a λ_{max} of 342 nm with similar Mie scattering to that observed in toluene solution at low temperatures. The emission profile of the aggregates closely matches that recorded at −90 °C in toluene solution, as well as the polycrystalline film and solid-state fluorescence spectra. Nonetheless, **1**, **2**, **4**, and **5** are stable in dry THF as evident by ^{1}H NMR studies in DCM-d_2 containing one drop of THF (Fig. S24–S27), which further implicates the stability of borenium ions owing to carbone coordination.

Expanding on our previous observations of thermochromic behavior in 3-methoxy-9-borafluorenium ions,[17] we then studied the temperature-dependent luminescence behavior of compound **5** in DCM (Fig. S47–S50). As the DCM solution of

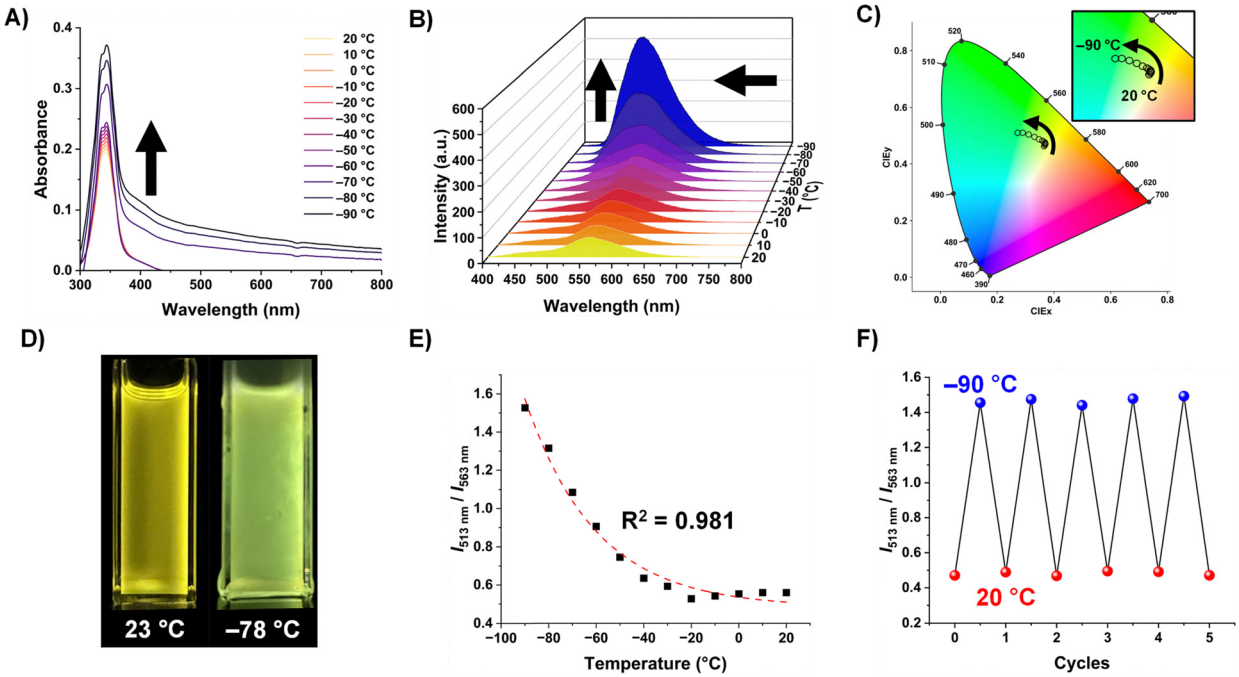

Fig. 6 (A) Variable temperature UV-vis spectra of **5** in toluene (0.01 mM). (B) Variable temperature fluorescence spectra of **5** in toluene (0.01 mM; λ_{ex} = 340 nm) (C) CIE (1931) chromaticity diagram of **5** in toluene (0.01 mM) at variable temperatures. Arrow shows trend as temperature decreases from 20 °C to −90 °C. (D) Images of **5** in toluene under 365 nm light at 23 °C (left) and −78 °C (right). (E) Plot and exponential curve fitting of fluorescence intensity ratio (I_{513nm}/I_{563nm}) *vs.* temperature (°C). (F) Reversible change in fluorescence intensity (I_{513nm}/I_{563nm}) observed over five temperature cycles between 20 °C and −90 °C. Arrows indicate how the feature change as the temperature decreases.

5 was cooled from 20 °C to −90 °C, a new signal was observed at 520 nm, which became more prominent as the solution was cooled to −90 °C and resembles that observed in the solid state (λ_{em} = 517 nm). However, the intensity of this peak is limited by the freezing point of DCM (−96.7 °C), as well as the high solubility of **5**. As a result, we then sought to assess the temperature-dependent characteristics of **5** in toluene, which is less polar and more viscous than DCM. The absorption profile of compound **5** in toluene (Fig. 6A) shows a λ_{max} of 342 nm at 20 °C. Gradual cooling of the solution of **5** results in an increase in absorbance (attributed to polarization effects),[102,103] as well as the observation of intensified absorption tails caused by Mie scattering,[102,103] a common phenomenon in compounds that exhibit AIE at lower energy wavelengths (Fig. 6A).[104] Because of the changes observed in the photoluminescence of **5** as a function of temperature in DCM, the emission profile of compound **5** in toluene (Fig. 6B) was assessed from 20 °C to −90 °C. At 20 °C, **5** exhibits an emission band at 563 nm. Upon incremental cooling to −50 °C, a shoulder peak at 513 nm, similar to that in DCM, was observed. Further cooling to −90 °C yielded a dominant peak at 513 nm, resulting in a stark color change from yellow (20 °C) to green (−90 °C) (Fig. 6C and D) and is in agreement with the solid-state fluorescence data. The thermochromic behavior of **5** was shown to be fully reversible by subjecting the solution to five cooling/warming cycles (Fig. 6F), which further highlights the stimuli-responsive behavior of this class of borenium ions.

Conclusion

We have reported the synthesis and optical properties of carbodiphosphorane-coordinated borafluorenium ions and further demonstrated a strategy for improving the stability cationic boracycles. Incorporation of 3,3′-dimethoxy substituents onto the aryl backbone of the borafluorene resulted in pronounced photostability and persistence in solution when compared to the unsubstituted species. By installing 3,3′-dimethoxy groups and changing the counteranion from Br^- to BAr^{F-}_4, differences in solution- and solid-state emission spectra were observed. The borafluorenium ions all exhibited pronounced AIE behavior with markedly high AIE factors. Detailed studies of **5** demonstrated that the AIE properties result in thermoluminescent behavior in toluene, wherein the emission is yellow at room temperature (λ_{em} = 563 nm, 20 °C) and green at low temperature (λ_{em} = 513 nm, −90 °C), which is in agreement with the solid-state and polycrystalline data. These results show that the choice of ligand can dictate the photophysical properties, such as the suppression of twisted intramolecular charge transfer processes, of borafluorenium ions. Further studies within our laboratory are underway to harness the stability and stimuli-responsive properties of carbone-ligated borenium ions.

Author contributions

The manuscript was written through contributions of all authors. All authors have given approval to the final version of the manuscript.

Conflicts of interest

There are no conflicts to declare.

Data availability

Experimental details, NMR spectra, photophysical data, single-crystal X-ray diffraction data, and computational details. See DOI: https://doi.org/10.1039/d5tc02785c

CCDC: 2466990 (**1**), 2466991 (**2**), 2441181 (**3**), 2441186 (**5**) contain the supplementary crystallographic data for this paper.[105a–d]

Acknowledgements

We are grateful to the National Science Foundation Chemical Synthesis (CHE 2046544) and Major Research Instrumentation (CHE 2018870) programs for support of this work. R. J. G. acknowledges additional laboratory support through a Beckman Young Investigator award from the Arnold & Mabel Beckman Foundation. N. C. F. acknowledges the National Science Foundation for a Graduate Research Fellowship (grant #1842490). K. K. H. acknowledges the American Association of University Women (AAUW) for a Dissertation Year Fellowship. The authors acknowledge the MIT Office of Research Computing and Data, MIT SuperCloud, and Lincoln Laboratory Supercomputing Center for providing resources that have contributed to the research results within this report.

Notes and references

1 Z. Yuan, N. J. Taylor, T. B. Marder, I. D. Williams, S. K. Kurtz and L.-T. Cheng, *J. Chem. Soc., Chem. Commun.*, 1990, 1489–1492, DOI: 10.1039/C39900001489.
2 Z. Yuan, N. J. Taylor, Y. Sun, T. B. Marder, I. D. Williams and C. Lap-Tak, *J. Organomet. Chem.*, 1993, **449**, 27–37.
3 Z. Yuan, N. J. Taylor, R. Ramachandran and T. B. Marder, *Appl. Organomet. Chem.*, 1996, **10**, 305–316.
4 Z. Yuan, J. C. Collings, N. J. Taylor, T. B. Marder, C. Jardin and J.-F. Halet, *J. Solid State Chem.*, 2000, **154**, 5–12.
5 H. Lee, D. Karthik, R. Lampande, J. H. Ryu and J. H. Kwon, *Front. Chem.*, 2020, **8**, 1–16.
6 K. R. Naveen, H. I. Yang and J. H. Kwon, *Commun. Chem.*, 2022, **5**, 149.
7 J. Shi, Z. Ran, F. Peng, M. Chen, L. Li, L. Ji and W. Huang, *J. Mater. Chem. C*, 2022, **10**, 9165–9191.
8 M. Du, J. Zhou, X. Luo, L. Duan and D. Zhang, *Moore and More*, 2024, **1**, 5.
9 M. Mamada, M. Hayakawa, J. Ochi and T. Hatakeyama, *Chem. Soc. Rev.*, 2024, **53**, 1624–1692.
10 S. Yamaguchi and A. Wakamiya, *Pure Appl. Chem.*, 2006, **78**, 1413–1424.
11 D. R. Levine and J. D. Tovar, *Polycyclic Arenes and Heteroarenes*, 2015, pp. 251–276, DOI: 10.1002/9783527689545.ch10.
12 A. Wakamiya and S. Yamaguchi, *Bull. Chem. Soc. Jpn.*, 2015, **88**, 1357–1377.
13 L. Ji, S. Griesbeck and T. B. Marder, *Chem. Sci.*, 2017, **8**, 846–863.
14 S. Mukherjee and P. Thilagar, *Main Group Strategies towards Functional Hybrid Materials*, 2017, pp. 27–45, DOI: 10.1002/9781119235941.ch2.
15 A. Wakamiya, *Main Group Strategies towards Functional Hybrid Materials*, 2017, pp. 1–26, DOI: 10.1002/9781119235941.ch1.
16 E. von Grotthuss, A. John, T. Kaese and M. Wagner, *Asian J. Org. Chem.*, 2018, **7**, 37–53.
17 W. Yang, K. E. Krantz, L. A. Freeman, D. A. Dickie, A. Molino, A. Kaur, D. J. D. Wilson and R. J. Gilliard Jr., *Chem. – Eur. J.*, 2019, **25**, 12512–12516.
18 K. K. Hollister, A. Molino, G. Breiner, J. E. Walley, K. E. Wentz, A. M. Conley, D. A. Dickie, D. J. D. Wilson and R. J. Gilliard, Jr., *J. Am. Chem. Soc.*, 2022, **144**, 590–598.
19 C.-L. Deng, A. D. Obi, B. Y. E. Tra, S. K. Sarkar, D. A. Dickie and R. J. Gilliard, *Nat. Chem.*, 2024, **16**, 437–445.
20 K. K. Hollister, A. Molino, V. V. Le, N. Jones, W. J. Smith, P. Müller, D. A. Dickie, D. J. D. Wilson and R. J. Gilliard, *Chem. Sci.*, 2024, **15**, 14358–14370.
21 H. Kim and R. J. Gilliard, Jr., *J. Am. Chem. Soc.*, 2025, **147**, 23213–23225.
22 K. K. Hollister, K. E. Wentz and R. J. Gilliard, Jr., *Acc. Chem. Res.*, 2024, **57**, 1510–1522.
23 E. Tsurumaki, S.-y Hayashi, F. S. Tham, C. A. Reed and A. Osuka, *J. Am. Chem. Soc.*, 2011, **133**, 11956–11959.
24 Y. Adachi, F. Arai and F. Jäkle, *Chem. Commun.*, 2020, **56**, 5119–5122.
25 B. D. Katzman, R. R. Maar, D. Cappello, M. O. Sattler, P. D. Boyle, V. N. Staroverov and J. B. Gilroy, *Chem. Commun.*, 2021, **57**, 9530–9533.
26 M. F. Silva Valverde, P. Schweyen, D. Gisinger, T. Bannenberg, M. Freytag, C. Kleeberg and M. Tamm, *Angew. Chem., Int. Ed.*, 2017, **56**, 1135–1140.
27 C. Chen, J. Li, C. G. Daniliuc, C. Mück-Lichtenfeld, G. Kehr and G. Erker, *Angew. Chem., Int. Ed.*, 2020, **59**, 21460–21464.
28 J. M. Farrell, D. Schmidt, V. Grande and F. Würthner, *Angew. Chem., Int. Ed.*, 2017, **56**, 11846–11850.
29 T. Heitkemper and C. P. Sindlinger, *Chem. – Eur. J.*, 2020, **26**, 11684–11689.
30 F. Ramirez, N. B. Desai, B. Hansen and N. McKelvie, *J. Am. Chem. Soc.*, 1961, **83**, 3539–3540.
31 C. A. Dyker, V. Lavallo, B. Donnadieu and G. Bertrand, *Angew. Chem., Int. Ed.*, 2008, **47**, 3206–3209.
32 O. Kaufhold and F. E. Hahn, *Angew. Chem., Int. Ed.*, 2008, **47**, 4057–4061.
33 S. Klein, R. Tonner and G. Frenking, *Chem. – Eur. J.*, 2010, **16**, 10160–10170.
34 W. Petz and G. Frenking, in *Transition Metal Complexes of Neutral eta1-Carbon Ligands*, ed. R. Chauvin and Y. Canac, Springer Berlin Heidelberg, Berlin, Heidelberg, 2010, pp. 49–92, DOI: 10.1007/978-3-642-04722-0_3.

35 G. Frenking and R. Tonner, *Wiley Interdiscip. Rev.: Comput. Mol. Sci.*, 2011, **1**, 869–878.
36 T.-H. Wang, W.-C. Chen and T.-G. Ong, *J. Chin. Chem. Soc.*, 2017, **64**, 124–132.
37 M. Alcarazo, in *Modern Ylide Chemistry: Applications in Ligand Design, Organic and Catalytic Transformations*, ed. V. H. Gessner, Springer International Publishing, Cham, 2018, pp. 25–50, DOI: 10.1007/430_2017_19.
38 S. Liu, W.-C. Chen and T.-G. Ong, in *Modern Ylide Chemistry: Applications in Ligand Design, Organic and Catalytic Transformations*, ed. V. H. Gessner, Springer International Publishing, Cham, 2018, pp. 51–71, DOI: 10.1007/430_2017_20.
39 S.-k Liu, W.-C. Shih, W.-C. Chen and T.-G. Ong, *ChemCatChem*, 2018, **10**, 1483–1498.
40 L. Zhao, C. Chai, W. Petz and G. Frenking, *Molecules*, 2020, **25**, 4943.
41 A. L. Liberman-Martin, *Cell Rep. Phys. Sci.*, 2023, **4**, 1–16.
42 F. Krischer and V. H. Gessner, *JACS Au*, 2024, **4**, 1709–1722.
43 B. Inés, M. Patil, J. Carreras, R. Goddard, W. Thiel and M. Alcarazo, *Angew. Chem., Int. Ed.*, 2011, **50**, 8400–8403.
44 W.-C. Chen, C.-Y. Lee, B.-C. Lin, Y.-C. Hsu, J.-S. Shen, C.-P. Hsu, G. P. A. Yap and T.-G. Ong, *J. Am. Chem. Soc.*, 2014, **136**, 914–917.
45 J. E. Münzer, P. Oña-Burgos, F. M. Arrabal-Campos, B. Neumüller, R. Tonner, I. Fernández and I. Kuzu, *Eur. J. Inorg. Chem.*, 2016, 3852–3858.
46 L. Xiang, J. Wang, W. Su, Z. Lin and Q. Ye, *Dalton Trans.*, 2021, **50**, 17491–17494.
47 L. Ding and Y. Fang, *Chem. Soc. Rev.*, 2010, **39**, 4258–4273.
48 X. Qian, Y. Xiao, Y. Xu, X. Guo, J. Qian and W. Zhu, *Chem. Commun.*, 2010, **46**, 6418–6436.
49 D. Yan, Z. Wang and Z. Zhang, *Acc. Chem. Res.*, 2022, **55**, 1047–1058.
50 L. Hu, Q. Zhang, X. Li and M. J. Serpe, *Mater. Horiz.*, 2019, **6**, 1774–1793.
51 X. Hou, C. Ke, C. J. Bruns, P. R. McGonigal, R. B. Pettman and J. F. Stoddart, *Nat. Commun.*, 2015, **6**, 6884.
52 Y. Shen, X. Le, Y. Wu and T. Chen, *Chem. Soc. Rev.*, 2024, **53**, 606–623.
53 Q. Guo, M. Zhang, Z. Tong, S. Zhao, Y. Zhou, Y. Wang, S. Jin, J. Zhang, H.-B. Yao, M. Zhu and T. Zhuang, *J. Am. Chem. Soc.*, 2023, **145**, 4246–4253.
54 W. Wang, Y. Zhou, L. Yang, X. Yang, Y. Yao, Y. Meng and B. Tang, *Adv. Funct. Mater.*, 2022, **32**, 2204744.
55 J. H. Day, *Chem. Rev.*, 1963, **63**, 65–80.
56 A. Hakami, S. S. Srinivasan, P. K. Biswas, A. Krishnegowda, S. L. Wallen and E. K. Stefanakos, *J. Coat. Technol. Res.*, 2022, **19**, 377–402.
57 Y. Hong, J. W. Y. Lam and B. Z. Tang, *Chem. Soc. Rev.*, 2011, **40**, 5361–5388.
58 C. Zhu, R. T. K. Kwok, J. W. Y. Lam and B. Z. Tang, *ACS Appl. Bio Mater.*, 2018, **1**, 1768–1786.
59 J. Mei, N. L. C. Leung, R. T. K. Kwok, J. W. Y. Lam and B. Z. Tang, *Chem. Rev.*, 2015, **115**, 11718–11940.
60 S. G. R. and A. S. J. Chakravarthy, *Mater. Chem. Front.*, 2021, **5**, 1541–1584.
61 Q. Wei, J. Zhang and Z. Ge, *Handbook of Aggregation-Induced Emission*, 2022, pp. 1–26, DOI: 10.1002/9781119643098.ch41.
62 Y. Duo, Z. Xiang, G. Gao, G. Luo and B. Z. Tang, *TrAC, Trends Anal. Chem.*, 2023, **167**, 117252.
63 Y. Zeng, D. Huang, B. Li, J. Wang and R. Hu, *Polym. Chem.*, 2025, **16**, 1897–1928.
64 Z. Zhao, J. W. Y. Lam and B. Z. Tang, *J. Mater. Chem.*, 2012, **22**, 23726–23740.
65 A. C. B. Rodrigues, M. Peixoto, C. Gomes, M. Pineiro and J. S. Seixas de Melo, *Chem. – Eur. J.*, 2022, **28**, e202103768.
66 Q. Li and L. Blancafort, *Chem. Commun.*, 2013, **49**, 5966–5968.
67 J. Chorbacher, J. Klopf, A. Friedrich, M. Fest, J. S. Schneider, B. Engels and H. Helten, *Angew. Chem., Int. Ed.*, 2025, **64**, e202416088.
68 M. Maier, J. Chorbacher, A. Hellinger, J. Klopf, J. Günther and H. Helten, *Chem. – Eur. J.*, 2023, **29**, e202302767.
69 R. Borthakur and V. Chandrasekhar, *Coord. Chem. Rev.*, 2021, **429**, 213647.
70 C. J. Berger, G. He, C. Merten, R. McDonald, M. J. Ferguson and E. Rivard, *Inorg. Chem.*, 2014, **53**, 1475–1486.
71 P. A. Chase, W. E. Piers and B. O. Patrick, *J. Am. Chem. Soc.*, 2000, **122**, 12911–12912.
72 S. Yamaguchi, T. Shirasaka, S. Akiyama and K. Tamao, *J. Am. Chem. Soc.*, 2002, **124**, 8816–8817.
73 A. Wakamiya, K. Mishima, K. Ekawa and S. Yamaguchi, *Chem. Commun.*, 2008, 579–581, DOI: 10.1039/B716107G.
74 D.-M. Chen, Q. Qin, Z.-B. Sun, Q. Peng and C.-H. Zhao, *Chem. Commun.*, 2014, **50**, 782–784.
75 M. F. Smith, S. J. Cassidy, I. A. Adams, M. Vasiliu, D. L. Gerlach, D. A. Dixon and P. A. Rupar, *Organometallics*, 2016, **35**, 3182–3191.
76 F. Rauch, S. Fuchs, A. Friedrich, D. Sieh, I. Krummenacher, H. Braunschweig, M. Finze and T. B. Marder, *Chem. – Eur. J.*, 2020, **26**, 12794–12808.
77 X. Chen, G. Meng, G. Liao, F. Rauch, J. He, A. Friedrich, T. B. Marder, N. Wang, P. Chen, S. Wang and X. Yin, *Chem. – Eur. J.*, 2021, **27**, 6274–6282.
78 Y. Li, X. Chen, W. Zhang, J. Zhang, L. Xu, Y. Qiao, K. Liu, N. Wang, P. Chen and X. Yin, *Org. Lett.*, 2021, **23**, 7236–7241.
79 S. Malzkuhn, X. Guo, D. Häussinger and O. S. Wenger, *J. Phys. Chem. A*, 2019, **123**, 96–102.
80 X. Su, T. A. Bartholome, J. R. Tidwell, A. Pujol, S. Yruegas, J. J. Martinez and C. D. Martin, *Chem. Rev.*, 2021, **121**, 4147–4192.
81 A. Hubner, H.-W. Lerner, M. Wagner and M. Bolte, *Acta Crystallogr., Sect. E: Struct. Rep. Online*, 2010, **66**, o444.
82 J. Wang, X. Gu, H. Ma, Q. Peng, X. Huang, X. Zheng, S. H. P. Sung, G. Shan, J. W. Y. Lam, Z. Shuai and B. Z. Tang, *Nat. Commun.*, 2018, **9**, 2963.
83 M. N. Berberan Santos, *PhysChemComm*, 2000, **3**, 18–23.
84 D. Ma, L. Duan, Y. Wei, L. He, L. Wang and Y. Qiu, *Chem. Commun.*, 2014, **50**, 530–532.
85 C. Wang, W. R. Kitzmann, F. Weigert, C. Förster, X. Wang, K. Heinze and U. Resch-Genger, *ChemPhotoChem*, 2022, **6**, e202100296.
86 J. C. Roberts and J. A. Pincock, *J. Org. Chem.*, 2006, **71**, 1480–1492.

87 M. Albrecht, C. Bohne, A. Granzhan, H. Ihmels, T. C. S. Pace, A. Schnurpfeil, M. Waidelich and C. Yihwa, *J. Phys. Chem. A*, 2007, **111**, 1036–1044.
88 A. Bucinskas, G. Bagdziunas, A. Tomkeviciene, D. Volynyuk, N. Kostiv, D. Gudeika, V. Jankauskas, M. Rutkis and J. V. Grazulevicius, *RSC Adv.*, 2015, **5**, 49577–49589.
89 V. Barone and M. Cossi, *J. Phys. Chem. A*, 1998, **102**, 1995–2001.
90 A. D. Becke, *J. Chem. Phys.*, 1993, **98**, 5648–5652.
91 C. Lee, W. Yang and R. G. Parr, *Phys. Rev. B: Condens. Matter Mater. Phys.*, 1988, **37**, 785–789.
92 S. Grimme, S. Ehrlich and L. Goerigk, *J. Comput. Chem.*, 2011, **32**, 1456–1465.
93 F. Weigend and R. Ahlrichs, *Phys. Chem. Chem. Phys.*, 2005, **7**, 3297–3305.
94 K. Chen, G. Li, H. Zhang, H. Wu, Y. Li, Y. Li, Z. Wang and B. Z. Tang, *Chem. Eng. J.*, 2022, **433**, 133646.
95 Q. Liu, K. Chen, Q. Deng, J. Li, Z. Wang and B. Z. Tang, *Adv. Opt. Mater.*, 2024, **12**, 2301903.
96 Y. Cai, L. Du, K. Samedov, X. Gu, F. Qi, H. H. Y. Sung, B. O. Patrick, Z. Yan, X. Jiang, H. Zhang, J. W. Y. Lam, I. D. Williams, D. Lee Phillips, A. Qin and B. Z. Tang, *Chem. Sci.*, 2018, **9**, 4662–4670.
97 N. L. C. Leung, N. Xie, W. Yuan, Y. Liu, Q. Wu, Q. Peng, Q. Miao, J. W. Y. Lam and B. Z. Tang, *Chem. – Eur. J.*, 2014, **20**, 15349–15353.
98 J. Chen, C. C. W. Law, J. W. Y. Lam, Y. Dong, S. M. F. Lo, I. D. Williams, D. Zhu and B. Z. Tang, *Chem. Mater.*, 2003, **15**, 1535–1546.
99 J. Chen, Z. Xie, J. W. Y. Lam, C. C. W. Law and B. Z. Tang, *Macromolecules*, 2003, **36**, 1108–1117.
100 J. Krebs, A. Häfner, S. Fuchs, X. Guo, F. Rauch, A. Eichhorn, I. Krummenacher, A. Friedrich, L. Ji, M. Finze, Z. Lin, H. Braunschweig and T. B. Marder, *Chem. Sci.*, 2022, **13**, 14165–14178.
101 H. Budy, T. Kaese, M. Bolte, H.-W. Lerner and M. Wagner, *Angew. Chem., Int. Ed.*, 2021, **60**, 19397–19405.
102 H. J. Egelhaaf, J. Gierschner, J. Haiber and D. Oelkrug, *Opt. Mater.*, 1999, **12**, 395–401.
103 H. J. Egelhaaf, J. Gierschner and D. Oelkrug, *Synth. Met.*, 2002, **127**, 221–227.
104 S. Pramanik, V. Bhalla and M. Kumar, *ACS Appl. Mater. Interfaces*, 2014, **6**, 5930–5939.
105 (*a*) N. C. Frey, K. K. Hollister, C. C. Taylor, N. Jones, D. A. Dickie and R. J. Gilliard Jr, 2466990: Experimental Crystal Structure Determination, DOI: **10.5517/ccdc.csd.cc2nt3by**; (*b*) N. C. Frey, K. K. Hollister, C. C. Taylor, N. Jones, D. A. Dickie and R. J. Gilliard Jr, 2466991: Experimental Crystal Structure Determination, DOI: **10.5517/ccdc.csd.cc2nt3cz**; (*c*) N. C. Frey, K. K. Hollister, C. C. Taylor, N. Jones, D. A. Dickie and R. J. Gilliard Jr, 2441181: Experimental Crystal Structure Determination, DOI: **10.5517/ccdc.csd.cc2my7sm**; (*d*) N. C. Frey, K. K. Hollister, C. C. Taylor, N. Jones, D. A. Dickie and R. J. Gilliard Jr, 2441186: Experimental Crystal Structure Determination, DOI: **10.5517/ccdc.csd.cc2my7ys**.